ADVANCED MATERIALS
www.advmat.de

A High Capacity Gas Diffusion Electrode for Li–O_2 Batteries

Max Jenkins, Daniel Dewar, Marco Lagnoni, Sixie Yang, Gregory J. Rees, Antonio Bertei, Lee R. Johnson, Xiangwen Gao, and Peter G. Bruce**

The very high theoretical specific energy of the lithium–air (Li–O_2) battery (3500 Wh kg^{-1}) compared with other batteries makes it potentially attractive, especially for the electrification of flight. While progress has been made in realizing the Li–air battery, several challenges remain. One such challenge is achieving a high capacity to store charge at the positive electrode at practical current densities, without which Li–air batteries will not outperform lithium-ion. The capacity is limited by the mass transport of O_2 throughout the porous carbon positive electrode. Here it is shown that by replacing the binder in the electrode by a polymer with the intrinsic ability to transport O_2, it is possible to reach capacities as high as 31 mAh cm^{-2} at 1 mA cm^{-2} in a 300 µm thick electrode. This corresponds to a positive electrode energy density of 2650 Wh L^{-1} and specific energy of 1716 Wh kg^{-1}, exceeding significantly Li-ion batteries and previously reported Li–O_2 cells. Due to the enhanced oxygen diffusion imparted by the gas diffusion polymer, Li_2O_2 (the product of O_2 reduction on discharge) fills a greater volume fraction of the electrode and is more homogeneously distributed.

1. Introduction

The lithium–air (Li–O_2) battery has a theoretical specific energy of 3500 Wh kg^{-1}, higher than any other rechargeable battery. Based on the advances in Li–O_2 batteries made in recent years, modelling shows that a 100 KWh Li–O_2 battery, including the balance of plant (all air/solvent handling) could achieve ≈650 Wh kg^{-1} compared with ≈300 Wh kg^{-1} projected for future Li-ion battery packs.[1,2] If developed it could impact on the electrification of flight. The Li–O_2 battery consists of a Li metal negative electrode and a porous carbon positive electrode. On discharge, Li^+ forms at the negative electrode and O_2 from the air is reduced at the positive electrode to form Li_2O_2. The processes are reversed on charging.

Significant challenges must be solved if the potential of the Li–O_2 battery is to be realized.[1] A long cycle-life lithium metal negative electrode must be developed, which is also a target for Li–sulfur batteries and for the next generation of Li-ion batteries.[3–5] The discharge product at the positive electrode, Li_2O_2, is an insulating solid, the formation of which can passivate the surface of the porous electrode.[6] This can be overcome by introducing redox mediating molecules that move the formation of Li_2O_2 on discharge and its oxidation on charge away from the surface and into the pores of the positive electrode.[7–12] While this works, there is a need to develop oxidation mediators that charge at lower voltages than those currently available. Cyclability is limited due to electrolyte degradation that occurs within a relatively small number of cycles when practical capacities are used. While solving the problems of cycling, electrolyte stability and low voltage oxidation mediators are important, their value will not be realized unless high capacities at practical rates of discharge can be achieved.[13] It is this challenge that we address here.

The use of the reduction mediator, 2,5-di-tert-butyl-1,4-benzoquinone (DBBQ),[7,14] avoids the formation of Li_2O_2 on the surface of the positive electrode and early cell death. On discharge, DBBQ is reduced at the electrode surface to $DBBQ^-$, which then reacts chemically with O_2 dissolved in the electrolyte to precipitate Li_2O_2 particles within the pores of the electrode. The kinetics of the DBBQ (electro)chemical reactions are fast so in a typical cell, the process limiting the capacity at practical rates of discharge becomes the mass transport of O_2 through the electrode from the electrode/gas interface.[15–17] Several strategies have been explored to enhance O_2 transport throughout the porous electrode. O_2 carrying additives and fluorinated

M. Jenkins, D. Dewar, M. Lagnoni, S. Yang, G. J. Rees, P. G. Bruce
Department of Materials
University of Oxford
Parks Road, Oxford OX1 3PH, UK
E-mail: peter.bruce@materials.ox.ac.uk
M. Lagnoni, A. Bertei
Department of Civil and Industrial Engineering
University of Pisa
Pisa 56122, Italy
L. R. Johnson
Nottingham Applied Materials and Interfaces Group
School of Chemistry
University of Nottingham
Nottingham NG7 2RD, UK
X. Gao
Future Battery Research Centre
Global institute of Future Technology
Shanghai Jiao Tong University
Shanghai 200240, China
E-mail: xiangwen.gao@sjtu.edu.cn
P. G. Bruce
Department of Chemistry
University of Oxford
Oxford OX1 3TA, UK

The ORCID identification number(s) for the author(s) of this article can be found under https://doi.org/10.1002/adma.202405715

DOI: 10.1002/adma.202405715

solvents have been used to increase the concentration of dissolved O_2 in the electrolyte.[18–22] Modifications to the pore structure and increasing the surface area of the positive electrode have also been explored.[23–27] Another method includes separating the oxygen transport pathways from Li^+ and electron transport pathways.[28–31] It is estimated that Li_2O_2 must occupy >40% of the volume of the positive electrode to achieve >1300 Wh kg^{-1} (based on positive electrode mass) and a value >650 Wh kg^{-1} for the whole system (including balance of plant), and no strategy has achieved this at practical rates (i.e., >1 mA cm^{-2}). In aqueous fuel cells, oxygen transport is achieved through the use of an electrode containing hydrophobic/hydrophilic regions that create channels for gas transport.[32–34] This strategy is not compatible with the use of highly wetting organic solvents.[1] High rate and power Li–O_2 cells will only be achieved if a gas diffusion electrode (GDE) capable of enhanced O_2 transport is realized.

Here we describe a GDE for the aprotic Li–O_2 cell with high O_2 transport by incorporating O_2 diffusion polymers into the electrode. This is achieved by replacing the standard electrode binder, PTFE, with a copolymer of 4,5-difluoro-2,2-bis(trifluoromethyl)−1,3-dioxole and tetrafluoroethylene, which has a high O_2 diffusivity.[35–38] The polymer also acts as a binder. The superior O_2 transport through the polymer ensures a more even oxygen delivery throughout the electrode and therefore a more homogeneous distribution of Li_2O_2 in the pores, rather than it being concentrated at the electrolyte/gas interface and resulting in pore clogging at that interface. We demonstrate a 300 µm thick electrode that can deliver a capacity of 31 mAh cm^{-2}, corresponding to a specific energy of 1716 Wh kg^{-1} (electrode + electrolyte + Li_2O_2) and energy density of 2650 Wh L^{-1} (electrode) at a rate of 1 mA cm^{-2}. These numbers may be compared with a typical Li-ion positive electrode, 670 Wh kg^{-1} (electrode + electrolyte) and 1440 Wh L^{-1}(electrode), calculated from a positive electrode with a typical thickness of 125 µm, delivering a capacity of 5 mAh cm^{-2} (220 mAh g^{-1}) at 3.6 V.

2. Results and Discussion

The voltage versus capacity profiles at three different current densities are shown in **Figure 1**, along with the corresponding energy density and specific energy plots. Details of the cell and electrochemical measurements are given in the Experimental Section. Partially pre-delithiated $LiFePO_4$ was employed as the counter electrode instead of lithium metal. This was to avoid the problems of Li reactivity with the electrolyte and electrolyte contamination, a strategy used previously in order to focus on investigating the positive electrode.[14] However, in practical Li–O_2 cells, a Li metal electrode protected from the liquid electrolyte solution (e.g., by a solid electrolyte membrane) is required to realize the maximum energy density possible.[3,39] The Li_XFePO_4 was on its voltage plateau at 3.45 V vs Li^+/Li, and had sufficient capacity to ensure it remained so on discharging the cell. The voltage is given here against Li^+/Li as the reference, and the volumetric/gravimetric energy densities are calculated based on the positive electrode volume and mass (including electrolyte and Li_2O_2), and the integrated area under the discharge curve on the Li^+/Li reference scale. The GDE is a porous composite of carbon (Ketjen Black) and the GDP, poly[4,5-difluoro-2,2-bis(trifluoromethyl)−1,3-dioxole-*co*-tetrafluoroethylene], which has the structural formula shown in Figure 1b, alongside the structure of PTFE for comparison. The GDP is 87 mol% dioxolane component and 13 mol% tetrafluoroethylene component. Although PTFE and the GDP are both fluoropolymers, PTFE is semi-crystalline in contrast to the GDP copolymer, which is amorphous and possesses fluorinated dioxolane rings. The rings in this amorphous polymer have a high barrier to rotation coupled with weak interchain interactions, resulting in a high fractional free volume between the polymer chains.[35,36] Diffusion of gases through such polymers relies on the gas molecules being transported between adjacent free-volume elements, which in the GDP are ≈5.9–6.4 Å in size, by the thermally activated segmental motion of the polymer chains.[35,36] Otherwise, the GDP has a similar oxidation stability window (Figure S1, Supporting Information), mechanical properties, such as tensile strength (Table S1, Supporting Information), and wettability with the electrolyte (Figure S2, Supporting Information) to that of PTFE. Scanning electron microscopy (SEM) images and fluorine energy-dispersive X-ray (EDX) spectroscopy maps of the cross-section of the GDE (Figure S3, Supporting Information), show that the polymer is evenly distributed throughout the electrode. Upon addition of an electrolyte, consisting of 1 M LiTFSI in 1,2-dimethoxyethane (DME) with 50 × 10^{-3} M 2,5-di-*tert*-butyl-1,4-benzoquinone (DBBQ) as a reduction mediator, to the GDE it expanded from a pristine thickness of ≈200–290 µm, as measured by a digital caliper. No further expansion occurred during the discharge process, regardless of the discharge capacity.

As shown in Figure 1a, at a rate of 1 mA cm^{-2} a capacity of 31 mAh cm^{-2} can be achieved, corresponding to a specific energy of 1716 Wh kg^{-1} for the porous positive electrode (electrode + electrolyte + Li_2O_2) and an energy density of 2650 Wh L^{-1} (electrode). This may be compared with a typical Li-ion positive electrode such as $LiNi_{0.8}Mn_{0.1}Co_{0.1}O_2$, which achieves 670 Wh kg^{-1} (electrode + electrolyte) and 1440 Wh L^{-1} (electrode), calculated from a positive electrode with a typical thickness of 125 µm with 20% porosity, delivering a capacity of 5 mAh cm^{-2} (220 mAh g^{-1}) at 3.6 V. As shown in Figure 1c,d, the specific energy and energy density of the GDE exceeds the typical Li-ion cathode at discharge rates up to 3 mA cm^{-2}. In addition, it exceeds previously reported energy densities for Li–O_2 cells at practical discharge rates (≥1 mA cm^{-2}), as shown in Table S2 in the Supporting Information.[13,14,40–43] Furthermore, the energy densities reported in the literature for Li–O_2 cells are based on the thickness of the porous electrode in the pristine state, and do not account for a decrease in energy density due to electrode expansion.

Powder X-ray diffraction (PXRD) and Fourier transform infrared (FTIR) data were collected from the electrode at the end of discharge (Figure 1e,f). In both cases the dominant phase present is Li_2O_2. The chemical analysis using titration by UV–vis/$TiOSO_4$ indicated a Li_2O_2 percentage yield of 85%, in good agreement with previous studies of Li–O_2 cells.[7,10,14] An SEM image taken of the GDE at the end of discharge shows the morphology of the Li_2O_2 grown within the porosity of the electrode (Figure S4, Supporting Information). By monitoring the pressure change in the head space above the cell during linear sweep voltammetry (LSV), the O_2 consumption during discharge gave an e^-/O_2 ratio of 2.02, in accord with the discharge reaction being $O_2 + 2e^- + 2Li^+ = Li_2O_2$ and demonstrating that the GDE does

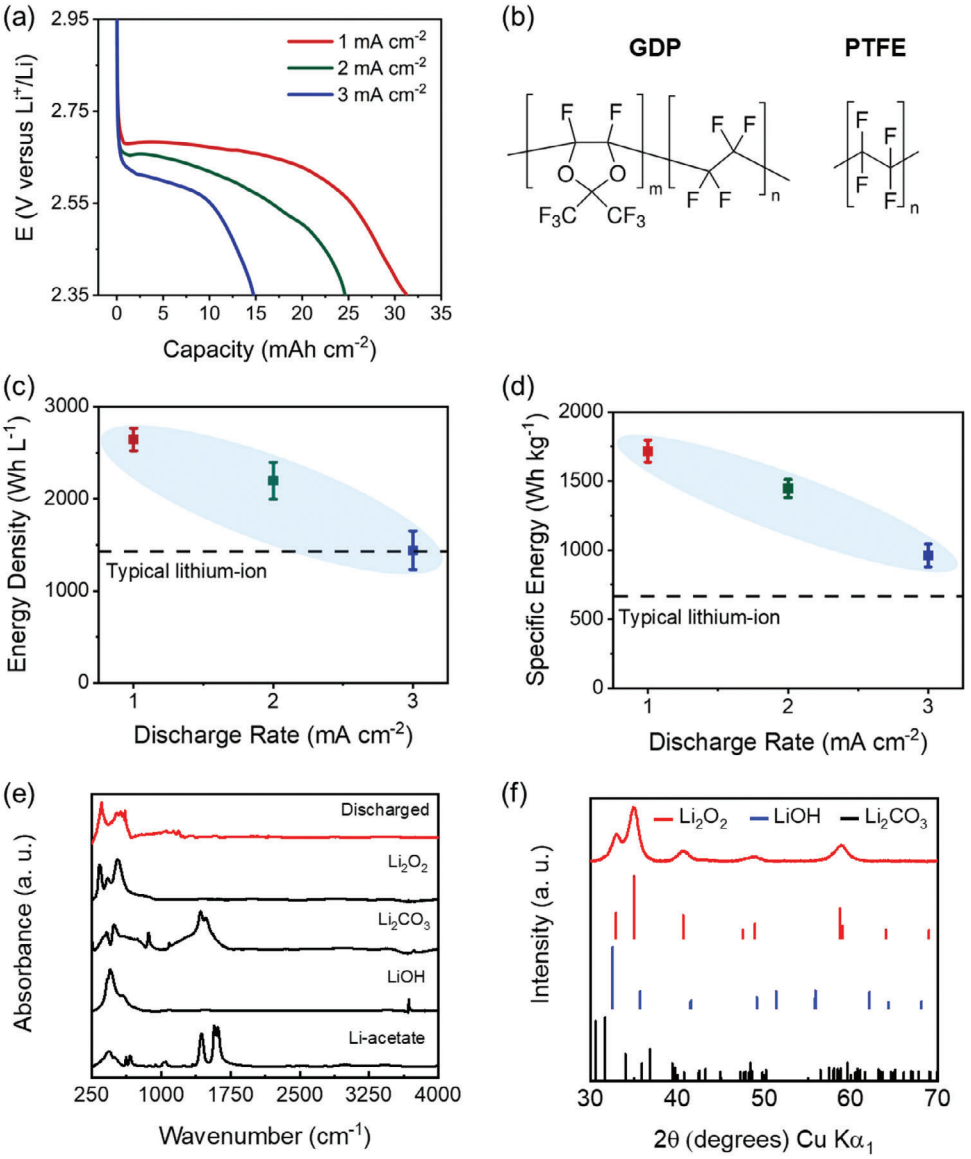

Figure 1. Electrochemical performance and product characterisation for the GDE. a) Load curves of oxygen reduction at a GDE fabricated from 60 wt.% Ketjen Black and 40 wt.% GDP. The cells are discharged in 1 M LiTFSI in DME with 50×10^{-3} M DBBQ at current densities from 1 to 3 mA cm^{-2} to a cut-off of 2.35 V. b) The chemical structure of the GDP, compared with PTFE. c) Energy density and d) specific energy plots for the GDEs discharged at different rates in (a). The dashed line represents the values for a typical lithium-ion electrode. The calculation was based on the integrated area under the discharge curve. e) XRD and f) FTIR spectra of the GDE discharged in 1 M LiTFSI in DME with 50×10^{-3} M DBBQ and under O_2.

not introduce any notable additional degradation (Figure S5, Supporting Information).[41,44,45]

The distribution of Li_2O_2 across the GDE from the gas interface towards the separator was determined at the end of discharge for each of the three current densities, as described in the Experimental Section. The electrodes after discharge were removed from the cell without the separator, and then washed and dried before assembling onto a microtome. 20 µm cross sections of the electrodes were taken using the microtome and the amount of Li_2O_2 in each was determined by titration with $TiOSO_4$ (**Figure 2a**). The results are shown in Figure 2b–d, where "depth into electrode" refers to the distance from the GDE/gas interface. At 1 mA cm^{-2}, Li_2O_2 is homogeneously distributed, with significant Li_2O_2 forming at the GDE/separator interface, rather than being concentrated at the electrode/gas interface as generally observed. As the current density increases, the quantity of Li_2O_2 forming in the region of the GDE/separator interface drops. The asymmetric distribution of Li_2O_2 towards the gas interface at higher current densities is in accord with the rate of discharge being limited by O_2 mass transport through the electrode.[16,46–49]

The effect of varying the composition of the porous GDE is presented in **Figure 3a,b**. The capacity and energy density of the discharged electrodes increase as the amount of GDP is increased, to a maximum at 40 wt.% GDP and thereafter drops significantly. The electronic conductivity of different wt.% GDP electrodes decreases with increased polymer loading, as shown in

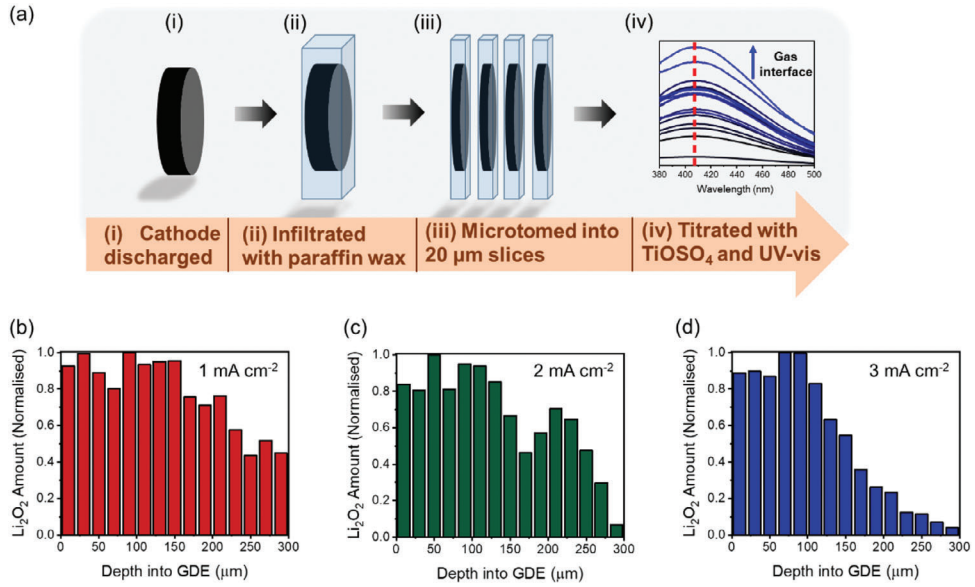

Figure 2. Measurement of the distribution of Li_2O_2 within the GDE after discharge. a) Outline of the method for depth-profiling the Li_2O_2 distribution in discharged GDEs. The discharged electrodes are infiltrated with paraffin wax, microtomed to 20 µm slices and the Li_2O_2 was determined by UV–vis titration with $TiOSO_4$. b–d) Distribution of Li_2O_2 across the electrodes measured from the GDE/gas interface to the GDE/electrolyte separator interface at 1, 2, 3 mA cm^{-2} (b, c, d respectively). The absorbances were normalized to the highest absorbance value measured in each electrode.

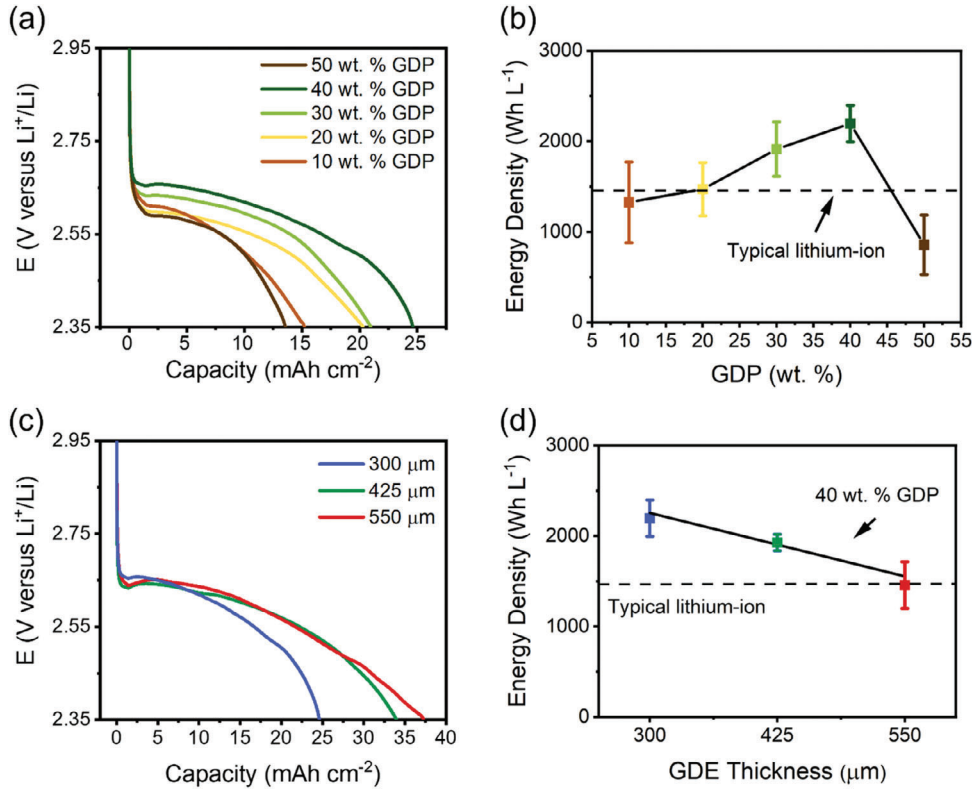

Figure 3. Impact of electrode composition and thickness on discharge capacity. a) Load curves of oxygen reduction at GDEs formed from Ketjen Black with various amounts of GDP (10–50 wt.%), electrodes otherwise identical. b) Energy densities of the GDEs shown in (a). c) Discharge load curves of a GDE fabricated from 40 wt.% GDP and Ketjen Black with electrode thicknesses of 300–550 µm (after discharge). d) Energy densities for the GDEs shown in (c). All discharge data shown were collected in 1 M LiTFSI in DME with 50×10^{-3} M DBBQ at current densities of 2 mA cm^{-2}.

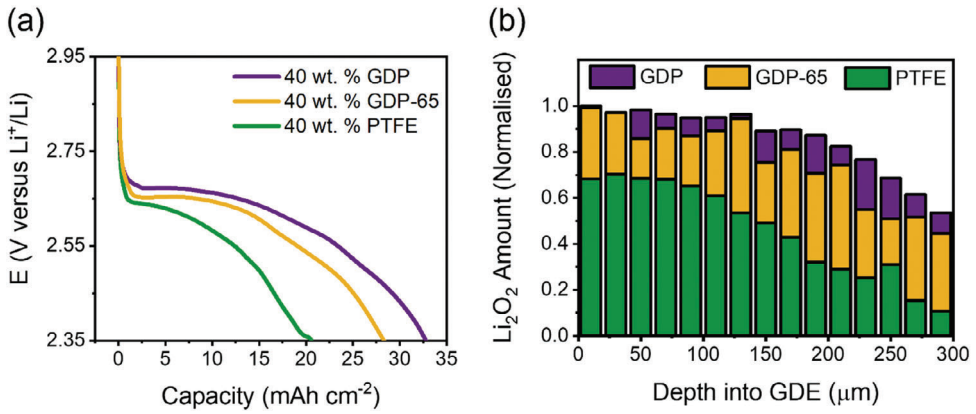

Figure 4. Impact of polymers with different O_2 permeability on cell capacity. a) Load curves for Ketjen Black electrodes with 40 wt.% gas diffusion polymer (GDP), 40 wt.% gas diffusion polymer-65 (GDP-65), or 40 wt.% PTFE. The GDEs are discharged in 1 M LiTFSI in DME with 50×10^{-3} M DBBQ at 1 mA cm^{-2} with a cut-off of 2.35 V. b) The distribution of Li_2O_2 at the end of discharge for the GDEs discharged in (a). The electrodes were microtomed into 20 μm slices and the Li_2O_2 content was determined by titration with $TiOSO_4$, normalized to the highest absorbance value measured.

Figure S6 (Supporting Information), which will act to hinder the discharge reaction. The 40 wt.% loading of GDP may represent a balance between sufficient carbon to ensure good electronic transport and sufficient GDP to ensure good O_2 transport.

Minimal changes in electrode porosity with increasing amounts of GDP were observed, as evidenced by the mercury intrusion porosimetry experiments in Figure S7 (Supporting Information), confirming that the increased discharge capacities are not due to any differences in the pore volume of the electrode. Because the cells were operated under a constant static pressure and there was no flowing O_2 gas, any improvements in O_2 mass transport are associated with the GDP. The effect of varying the thickness of the electrode is considered in Figure 3c,d. The small differences in voltage seen at the initial point of discharge may reflect changes in the electrolyte resistance that result from a thicker electrode. The final areal capacity increases with increasing thickness, but the benefit of this is more than offset by the increasing electrode volume, as is reflected in the values for the energy density as a function of electrode thickness in Figure 3d.

The GDP was used because of its enhanced O_2 transport properties. We compared this GDE with porous positive electrodes based on the same carbon but using the widely employed polymer binder in Li–O_2 cells, PTFE, itself of course a fluorinated hydrocarbon. We also compared this to a second gas diffusion polymer, GDP-65 with an O_2 permeability between GDP and PTFE. All have similar mechanical properties (Table S1, Supporting Information) but the O_2 permeabilities of the different polymers are 99 000 cB (GDP), 34 000 cB (GDP-65), and 420 cB (PTFE).[38,50] GDP-65 has the same structure as the GDP used in this work, but with a lower ratio of dioxolane to perfluorinated alkane component (65 vs 87 mol%), resulting in a lower oxygen permeability, and thus we would expect a lower capacity if the solid-state gas diffusion is responsible for the performance improvement. The comparison of the electrodes with different polymers is shown in **Figure 4**. All the electrodes have the same mass fraction of polymer and thickness. The highest capacity is obtained with the GDP electrode, which has the highest O_2 permeability, and the lowest is for PTFE with the GDP-65 providing a capacity in between the two. The commonly used composition for PTFE electrodes is a 90:10 mass ratio of carbon: PTFE.[51,52] Changing this ratio in the PTFE-based electrode does not cause the electrode porosity or deep discharge capacity to change notably (Figures S7 and S8, Supporting Information). The 40 wt.% GDP electrode outperforms all PTFE-based electrodes regardless of the wt.% of PTFE included. The observation that a higher proportion of polymer is only advantageous when the polymer can transport O_2 is in accord with O_2 transport through the electrode being rate limiting.

The distributions of Li_2O_2 across the three electrodes, containing GDP, GDP-65 or PTFE, are compared in Figure 4b. When using PTFE, the amount of Li_2O_2 stored in the electrode drops markedly away from the GDE/gas interface. PTFE is a semi-crystalline polymer with a low fraction of amorphous phase and low fractional free volume which results in its low oxygen permeability (420 cB).[53] In comparison, a more even distribution of Li_2O_2 is found when using either GDP, which both support superior O_2 diffusion. The increasing homogeneity of the Li_2O_2 distribution is in agreement with the trend in the O_2 permeability of the polymers: GDP (99 000 cB) > GDP-65 (34 000 cB) > PTFE (420 cB).

To further demonstrate the superior O_2 transport through the composite cathode containing the GDP, cyclic voltammetry (CV) of the cathodes with 40 wt.% GDP and PTFE were performed in the cell under an O_2 atmosphere and the O_2 consumption measured by in situ monitoring of the gas pressure (Figure S9, Supporting Information). The scan rate (0.1 mV s^{-1}) was chosen so that the cathodic charge passed in the CV was comparable to that obtained during cell discharge. These results were compared to a CV performed in an Ar environment, which confirmed that the GDP/electrolyte was stable within the relevant electrochemical window (Figure S9a, Supporting Information). During the cathodic sweep in the O_2 environment, the peak reduction current was larger in the cell containing 40 wt.% GDP compared to 40 wt.% PTFE. Commensurately, the amount of charge passed and O_2 consumed in the cell with the GDP were both 42% larger compared to the PTFE cathode (Figure S9b, Supporting Information). Since both cathodes have the same geometric surface area,

thickness and mass-loading of carbon, this confirms enhanced transport of the limiting-reactant for the discharge reaction (i.e., O_2) when the GDP is included.

A modelling study was carried out to complement the experimental evidence which shows that an O_2 permeable binder can increase O_2 transport throughout the composite cathode and enable a more homogeneous Li_2O_2 distribution. In the model, O_2 is converted to Li_2O_2 through a first-order homogeneous reaction with respect to O_2 concentration, representing the reaction that takes place in the cathode pores due to the use of the reduction mediator in the cells. Using Fick's law, the O_2 molar flux is defined with an effective diffusion coefficient ($D_{O_2,\text{eff}}$) that incorporates the electrode's microstructure and material composition. The theoretical model indicates that $D_{O_2,\text{eff}}$ of the electrode is enhanced by a factor of 6 when the electrode contains 40 wt.% GDP compared to an equivalent cathode with PTFE. Details of the model and the calculation are given in Note S1 in the Supporting Information.

Because the cell-level energy density obtained in Swagelok/coin/pouch cells is not representative of the energy density of a realistic Li–air system, a modified version of the BatPac software was used to predict the energy density of a realistic Li–air battery that uses the GDP.[54] Taking the cathodic specific energy of the 40 wt.% GDP electrode after deep discharge at 1 mA cm^{-2}, we consider a bipolar cell that utilizes a ceramic separator to protect the Li metal negative electrode with an additional liquid electrolyte separator based on polypropylene. Values of 650 Wh L^{-1} and 595 Wh kg^{-1} are predicted for a full Li–air system of 100 KWh. The details are given in Table S3 in the Supporting Information. This value includes the mass and volume of all air and solvent-handling components rated at 50 kg and 50 L, which would be required if volatile solvents like DME were to be used.[54]

This work tackles the challenge of boosting the O_2 transport in the cathode, leading to high capacities at high discharge currents in Li–O_2 cells. Charging is a different problem that requires discovery of new low voltage oxidation mediators that oxidize the Li_2O_2, and efficient cycling will require a solution to the problem of degradation.[55,56] These problems are illustrated in the cycling of a 40 wt.% GDP electrode with the addition of the charging mediator TEMPO (Figure S10, Supporting Information).[7,11] Within only a few cycles, the discharge and charge polarization increases due to a build-up of passivating products in the electrode.[57,58] The stability of the GDP during cycling was confirmed by performing solid state ^{19}F NMR on the cycled GDE from this cell. This was compared to a control GDE which was assembled in a cell but not cycled (Figure S11, Supporting Information). No new fluorine containing side-products were identifiable after cycling the cell, suggesting that the GDP does not introduce a new source of degradation in Li–O_2 cells.

3. Conclusions

By replacing PTFE, which is widely used as the binder in the positive electrodes of Li–O_2 cells, with a polymer capable of transporting O_2, a discharge capacity of 31 mAh cm^{-2} at a rate of 1 mA cm^{-2} was achieved, which corresponds to an energy density of 2650 Wh L^{-1} and a specific energy of 1716 Wh kg^{-1}. The gas diffusion electrode is composed of Ketjen Black and the co-polymer poly[4,5-difluoro-2,2-bis(trifluoromethyl)−1,3-dioxole-*co*-tetrafluoroethylene], with an O_2 permeability of 99 000 cB compared with 420 cB for PTFE. The gas diffusion polymer results in a more even distribution of Li_2O_2 within the electrode compared to cells which utilize standard PTFE as the binder. The higher capacity obtained with the gas diffusion polymer exceeds those reported previously for Li–O_2 and Li-ion positive electrodes at comparable rates. While the higher discharge capacity at practical rates demonstrated here does not address all the challenges facing the Li–air cell, including degradation, a protected lithium metal anode, and operation in air (i.e., a need to reduce the CO_2 and H_2O content in the gas stream), it represents a significant advance in one of the important challenges facing the Li–air battery.

4. Experimental Section

Electrode Fabrication: The as-received Ketjen Black EC600-JD (KB) (MSE Supplies) was ground into a fine powder before treating with Ar/H_2 at 900 °C to remove any reactive groups on the carbon surfaces.[59] The electrode composed of KB and the gas diffusion polymer, poly[4,5-difluoro-2,2-bis(trifluoromethyl)−1,3-dioxole-*co*-tetrafluoroethylene] (Sigma), was prepared by dissolving the latter in dry perfluoro(methylcyclohexane) (Sigma, technical grade). KB was then added to the solution and stirred at 70 °C until dry, then further dried under vacuum. The resulting mixture was weighed out (2 mg, 10 mg cm^{-2}) and pressed into 5 mm diameter disks (area = 0.2 cm^2) at 250 MPa. KB/PTFE electrodes were prepared by following a widely used procedure involving mixing KB with the desired amount of PTFE (Sigma) and making up to 15 mL with 4:1 MilliQ water to IPA solution.[49,51,60,61] The resulting mixture was stirred at 70 °C until dry under high vacuum. The resulting KB/PTFE was the weighed out (2 mg, 10 mg cm^{-2}) and pressed into 5 mm diameter disks (area = 0.2 cm^2) at 250 MPa. The thickness of the GDE was measured before and after electrolyte addition and after discharge using a digital caliper (RS Pro, 0.01 mm resolution).

Electrochemical Measurements: Electrochemical measurements were carried out using a Swagelok-type cell as described in detail previously.[7,14] $LiFePO_4$ electrodes were used as the negative electrode in place of Li. They were partially chemically delithiated using acetic acid (Sigma, >99%) and 30% w/w H_2O_2 (Sigma) so that 80% of the total maximum capacity remained. The $LiFePO_4$ electrodes were fabricated to have at least 120% of the maximum capacity that the positive electrode obtained on discharge. 1 M LiTFSI (Sigma, 99.95%) in 1,2-dimethoxyethane (DME, Sigma, 99.9%) with 50×10^{-3} M 2,5-di-tert-butyl-1,4-benzoquinone (DBBQ, Sigma, 99%) was used as the electrolyte (250 µL).[7] DME was dried over molecular sieves to <10 ppm H_2O prior to use. For the cell cycling experiment, 50×10^{-3} M of 2,2,6,6-tetramethylpiperidine 1-oxyl (TEMPO, Sigma, 99%) was added to the electrolyte. Electrochemical measurements were carried out using a Biologic VMP3 Multichannel Potentiostat. Prior to discharge, the cells were purged with oxygen (BOC, zero grade) through a Big Moisture Trap (Agilent). The cells were sealed and cycled as a closed system to avoid any loss of DME from the electrolyte solution. The cells were allowed to equilibrate for 3 h and then discharged at a temperature of 20 °C. An average performance was taken of three cells and one standard deviation was used.

The electrical conductivity of different wt.% GDP cathodes was measured by clamping the cathodes between two solid stainless steel electrodes and applying a 50 mV voltage.

Characterization Methods: Scanning electron microscopy (SEM) imaging and energy-dispersive X-ray (EDX) spectroscopy were carried out on a Zeiss Merlin. Powder X-ray diffraction (PXRD) data were collected with a Rigaku MiniFlex diffractometer with Cu $K_{\alpha 1}$ inside a N_2-filled glovebox. Samples were washed and dried using DME and were loaded onto a low-background silicon holder. Fourier transform infrared (FTIR) spectra were collected on a Nicolet 6700 spectrometer (Thermo Fischer Scientific)

in a N_2-filled glovebox and using a CsI beamsplitter. Samples were ground in a pestle and mortar with CsI and formed into a pellet using a die set and hydraulic press. Spectra were collected in transmission mode between 250 and 4000 cm^{-1}. Contact angle measurements were performed using films of either PTFE (Sigma) or the GDP. The GDP film was made by dissolving the polymer in perfluoro(methylcyclohexane) and then casting in a petri-dish by allowing the solvent to evaporate. For pressure cell measurements, a pressure transducer (Omega Engineering) was connected to the head space of a cell with 40 wt.% GDP or 40 wt.% PTFE as the GDE, to monitor the change in pressure during linear sweep voltammetry (LSV) or cyclic voltammetry (CV). The electrolyte was 50×10^{-3} M DBBQ in 1 M LiTFSI in DME. The cells were assembled in an Ar-filled glovebox and purged with O_2 through a Big Moisture Trap (Agilent). The cell was allowed to equilibrate for 6 h at 25 °C in a controlled temperature chamber (Labcold) to avoid any pressure change due to temperature fluctuation.[62] The voltage was swept at 0.1 mV s^{-1} from open circuit potential. From the known internal cell volume (5 mL), the pressure decrease in the head-space of the cell was used to calculate the moles of gas consumed by assuming an ideal-gas. The quantity of Li_2O_2 was determined by titration with $TiOSO_4$/1 M H_2SO_4 solution and measured by UV–vis spectroscopy using an Evolution 220 spectrophotometer (Thermo Scientific) as reported previously.[14]

To determine the distribution of Li_2O_2 across the electrode, the electrode was sliced by a microtome and the Li_2O_2 analyzed by UV–vis titration. The discharged electrode was washed and dried using DME. The extracted electrode was placed in a ParaFree Metal Base Mold 15×15×4 mm (TAAB) and infiltrated with molten paraffin wax (Paraplast X-TRA, Merck) under vacuum and affixed to a cassette (TAAB). The sample was cooled to (−10 °C) before taking 20 µm cross-sections using a RM2125 RTS microtome (Leica Biosystems). The expected error on each slice is ± 1 µm or ± 5%, based on the analogue error of the microtome which can be adjusted in 2 µm increments. Each cross-section was submerged in a known volume of 7.5% $TiOSO_4/H_2SO_4$ solution. UV–vis data was collected with an Evolution 220 spectrophotometer (Thermo Scientific). Li_2O_2 content was quantified by comparing the absorbance to a calibration curve of known Li_2O_2 concentration.

Mercury intrusion porosimetry was carried out on an Autopore IV 9500 (Micromeritics). The samples were dried under vacuum at 70 °C overnight before transferring to a 3 cc penetrometer (Micromeritics). Porosimetry was carried out between 14.7 psia (pounds per square inch absolute) to 33000 psia corresponding to pores between 100 µm and 6 nm.

Solid-state nuclear magnetic resonance (NMR) analysis was carried out at room temperature (298.15 K) on a Bruker Avance III HD 9.45 T spectrometer, operating at a Larmor frequency of (ν_0 [^{19}F] =) 376.6 MHz. The data was obtained at the magic angle spinning frequency (ν_R =) of 37 037 Hz ($\tau = 27$ µs) using a 1.9 mm Bruker probe-head. The respective chemical shift ranges were referenced against pure PTFE powder (δ_{iso} (^{19}F) = −124 ppm). The "before" and "after" cycling cathodes were washed with DME and dried under vacuum prior to measurement.

Supporting Information

Supporting Information is available from the Wiley Online Library or from the author.

Acknowledgements

P.G.B. is indebted to the EPSRC, including the SUPERGEN programme and the Henry Royce Institute for Advanced Materials (EP/R00661X/1, EP/S019367/1, EP/ R010145/1, EP/L019469/1) for financial support.

Conflict of Interest

The authors declare no conflict of interest.

Author Contributions

M.J. fabricated GDEs and carried out electrochemical measurements and designed and carried out experiments for lithium peroxide depth profiling and mercury intrusion porosimetry. M.J. characterized discharged electrodes with contributions from S.Y. D.D. performed pressure cell, contact angle and conductivity measurements and analyzed the data. G.R. performed solid state NMR measurements and analyzed the data. M.J., D.D., A.B., M.L. analyzed data. P.G.B., X.G., M.J., and D.D. interpreted the data. X.G. and P.G.B. wrote the manuscript with contributions from D.D., L.R.J., and M.J.

Data Availability Statement

The data that support the findings of this study are available from the corresponding author upon reasonable request.

Keywords

gas diffusion electrode, high energy density, lithium-oxygen battery

Received: April 22, 2024
Revised: July 15, 2024
Published online:

[1] W.-J. Kwak, D. S. Rosy, C. Xia, H. Kim, L. R. Johnson, P. G. Bruce, L. F. Nazar, Y.-K. Sun, A. A. Frimer, M. Noked, S. A. Freunberger, D. Aurbach, *Chem. Rev.* **2020**, *120*, 6626.
[2] M. M. Thackeray, C. Wolverton, E. D. Isaacs, *Energy Environ. Sci.* **2012**, *5*, 7854.
[3] C. Yan, X. Q. Zhang, J. Q. Huang, Q. Liu, Q. Zhang, *Trends Chem.* **2019**, *1*, 693.
[4] A. Manthiram, X. Yu, S. Wang, *Nat. Rev. Mater.* **2017**, *2*, 16103.
[5] X. X. Wang, D. H. Guan, C. L. Miao, D. C. Kong, L. J. Zheng, J. J. Xu, *J. Am. Chem. Soc.* **2023**, *145*, 5718.
[6] L. N. Song, L. J. Zheng, X. X. Wang, D. C. Kong, Y. F. Wang, Y. Wang, J. Y. Wu, Y. Sun, J. J. Xu, *J. Am. Chem. Soc.* **2024**, *146*, 1305.
[7] X. Gao, Y. Chen, L. R. Johnson, Z. P. Jovanov, P. G. Bruce, *Nat. Energy* **2017**, *2*, 17118.
[8] Y. Zhang, L. Wang, X. Zhang, L. Guo, Y. Wang, Z. Peng, *Adv. Mater.* **2018**, *30*, 1705571.
[9] Y. Ko, H. Park, J. Kim, H. D. Lim, B. Lee, G. Kwon, S. Lee, Y. Bae, S. K. Park, K. Kang, *Adv. Funct. Mater.* **2019**, *29*, 1805623.
[10] X. Bin Han, S. Ye, *ACS Catal.* **2020**, *10*, 9790.
[11] B. J. Bergner, A. Schürmann, K. Peppler, A. Garsuch, J. Janek, *J. Am. Chem. Soc.* **2014**, *136*, 15054.
[12] Y. Chen, S. A. Freunberger, Z. Peng, O. Fontaine, P. G. Bruce, *Nat. Chem.* **2013**, *5*, 489.
[13] A. Nomura, E. Mizuki, K. Ito, Y. Kubo, T. Yamagishi, M. Uejima, *Electrochim. Acta* **2021**, *400*, 139415.
[14] X. Gao, Y. Chen, L. Johnson, P. G. Bruce, *Nat. Mater.* **2016**, *15*, 882.
[15] Z. Su, V. De Andrade, S. Cretu, Y. Yin, M. J. Wojcik, A. A. Franco, *ACS Appl. Energy Mater.* **2020**, *3*, 4093.
[16] S. H. Park, Y. J. Cheon, Y. J. Lee, K. H. Shin, Y. Y. Hwang, Y. S. Jeong, Y. J. Lee, *ACS Appl. Mater. Interfaces* **2019**, *11*, 30872.
[17] M. Augustin, P. E. Vullum, F. Vullum-Bruer, A. M. Svensson, *J. Power Sources* **2019**, *414*, 130.
[18] M. Balaish, Y. Ein-Eli, *ACS Appl. Mater. Interfaces* **2017**, *9*, 9726.
[19] M. Balaish, Y. Ein-Eli, *J. Mater. Chem. A* **2017**, *5*, 14152.
[20] M. Balaish, Y. Ein-Eli, *J. Power Sources* **2018**, *378*, 219.
[21] M. Balaish, X. Gao, P. G. Bruce, Y. Ein-Eli, *Adv. Mater. Technol.* **2019**, *4*, 1800645.

[22] R. N. Samajdar, S. M. George, A. J. Bhattacharyya, *J. Phys. Chem. C* **2019**, *123*, 23433.
[23] S. Meini, M. Piana, H. Beyer, J. Schwämmlein, H. A. Gasteiger, *J. Electrochem. Soc.* **2012**, *159*, A2135.
[24] F. Wang, P. K. Kahol, R. Gupta, X. Li, *J. Electrochem. Energy Convers. Storage* **2019**, *16*, 041007.
[25] S. B. Ma, D. J. Lee, V. Roev, D. Im, S.-G. Doo, *J. Power Sources* **2013**, *244*, 494.
[26] Z. Guo, D. Zhou, X. Dong, Z. Qiu, Y. Wang, Y. Xia, *Adv. Mater.* **2013**, *25*, 5668.
[27] H. Nie, Y. Zhang, J. Li, W. Zhou, Q. Lai, T. Liu, H. Zhang, *RSC Adv.* **2014**, *4*, 17141.
[28] Z. Huang, Z. Deng, Y. Shen, W. Chen, W. Liu, M. Xie, Y. Li, Y. Huang, *J. Mater. Chem. A* **2019**, *7*, 3000.
[29] C. Chen, S. Xu, Y. Kuang, W. Gan, J. Song, G. Chen, G. Pastel, B. Liu, Y. Li, H. Huang, L. Hu, *Adv. Energy Mater.* **2019**, *9*, 1802964.
[30] S. Xu, Y. Yao, Y. Guo, X. Zeng, S. D. Lacey, H. Song, C. Chen, Y. Li, J. Dai, Y. Wang, Y. Chen, B. Liu, K. Fu, K. Amine, J. Lu, L. Hu, *Adv. Mater.* **2018**, *30*, 1704907.
[31] H. Song, S. Xu, Y. Li, J. Dai, A. Gong, M. Zhu, C. Zhu, C. Chen, Y. Chen, Y. Yao, B. Liu, J. Song, G. Pastel, L. Hu, *Adv. Energy Mater.* **2018**, *8*, 1701203.
[32] J. Park, H. Oh, T. Ha, Y. Il Lee, K. Min, *Appl. Energy* **2015**, *155*, 866.
[33] S. Shimpalee, U. Beuscher, J. W. Van Zee, *Electrochim. Acta* **2007**, *52*, 6748.
[34] T. Chen, S. Liu, J. Zhang, M. Tang, *Int. J. Heat Mass Transf.* **2019**, *128*, 1168.
[35] V. P. Shantarovich, I. B. Kevdina, Y. P. Yampolskii, A. Y. Alentiev, *Macromolecules* **2000**, *33*, 7453.
[36] A. Y. Alentiev, Y. P. Yampolskii, V. P. Shantarovich, S. M. Nemser, N. A. Plate, *J. Membr. Sci.* **1997**, *126*, 123.
[37] I. Pinnau, L. G. Toy, *J. Membr. Sci.* **1996**, *109*, 125.
[38] V. I. Bonder, B. D. Freeman, Y. P. Yampolskii, *Macromolecules* **1999**, *32*, 6163.
[39] B. J. Bergner, M. R. Busche, R. Pinedo, B. B. Berkes, D. Schröder, J. Janek, *ACS Appl. Mater. Interfaces* **2016**, *8*, 7756.
[40] S. Miyakawa, M. Goto, M. Ono, T. Saito, S. Yamaguchi, S. Matsuda, *ACS Appl. Energy Mater.* **2023**, *6*, 1906.
[41] T. Liu, J. T. Frith, G. Kim, R. N. Kerber, N. Dubouis, Y. Shao, Z. Liu, P. C. M. M. Magusin, M. T. L. Casford, N. Garcia-Araez, C. P. Grey, *J. Am. Chem. Soc.* **2018**, *140*, 1428.
[42] Z. L. Wang, D. Xu, J. J. Xu, L. L. Zhang, X. B. Zhang, *Adv. Funct. Mater.* **2012**, *22*, 3699.
[43] G. Oh, S. Seo, W. Kim, Y. Cho, H. Kwon, S. Kim, S. Noh, E. Kwon, Y. Oh, J. Song, J. Lee, K. Ryu, *ACS Appl. Mater. Interfaces* **2021**, *13*, 13200.
[44] A. Dutta, R. A. Wong, W. Park, K. Yamanaka, T. Ohta, Y. Jung, H. R. Byon, *Nat. Commun.* **2018**, *9*, 680.
[45] M. Ue, H. Asahina, S. Matsuda, K. Uosaki, *RSC Adv.* **2020**, *10*, 42971.
[46] S. D. Beattie, D. M. Manolescu, S. L. Blair, *J. Electrochem. Soc.* **2009**, *156*, A44.
[47] B. D. Adams, C. Radtke, R. Black, M. L. Trudeau, K. Zaghib, L. F. Nazar, *Energy Environ. Sci.* **2013**, *6*, 1772.
[48] B. Horstmann, B. Gallant, R. Mitchell, W. G. Bessler, Y. Shao-Horn, M. Z. Bazant, *J. Phys. Chem. Lett.* **2013**, *4*, 4217.
[49] J. Read, K. Mutolo, M. Ervin, W. Behl, J. Wolfenstine, A. Driedger, D. Foster, *J. Electrochem. Soc.* **2003**, *150*, A1351.
[50] S. Sunshine, Method for Extracting Gases Dissolved in a Liquid, International Patent WO, **1998**, *98*, 35739.
[51] J. Read, *J. Electrochem. Soc.* **2002**, *149*, A1190.
[52] U. Ulissi, G. A. Elia, S. Jeong, J. Reiter, N. Tsiouvaras, S. Passerini, J. Hassoun, *Chem. – Eur. J.* **2018**, *24*, 3178.
[53] G. Dlubek, K. Saarinen, H. M. Fretwell, *J. Polym. Sci., Part B: Polym. Phys.* **1998**, *36*, 1513.
[54] K. G. Gallagher, S. Goebel, T. Greszler, M. Mathias, W. Oelerich, D. Eroglu, V. Srinivasan, *Energy Environ. Sci.* **2014**, *7*, 1555.
[55] S. Ahn, C. Zor, S. Yang, M. Lagnoni, D. Dewar, T. Nimmo, C. Chau, M. Jenkins, A. J. Kibler, A. Pateman, G. J. Rees, X. Gao, P. Adamson, N. Grobert, A. Bertei, L. R. Johnson, P. G. Bruce, *Nat. Chem.* **2023**, *15*, 1022.
[56] X. Yao, Q. Dong, Q. Cheng, D. Wang, *Angew. Chem., Int. Ed.* **2016**, *55*, 11344.
[57] M. Jenkins, D. Dewar, T. Nimmo, C. Chau, X. Gao, P. G. Bruce, *Faraday Discuss.* **2023**, *248*, 318.
[58] Z. Zhao, J. Huang, Z. Peng, *Angew. Chem., Int. Ed.* **2018**, *57*, 3874.
[59] M. M. O. Thotiyl, S. A. Freunberger, Z. Peng, P. G. Bruce, *J. Am. Chem. Soc.* **2013**, *135*, 494.
[60] S. S. Zhang, D. Foster, J. Read, *J. Power Sources* **2010**, *195*, 1235.
[61] J. Read, *J. Electrochem. Soc.* **2006**, *153*, A96.
[62] F. Lepoivre, A. Grimaud, D. Larcher, J.-M. Tarascon, *J. Electrochem. Soc.* **2016**, *163*, A923.